Biomedical Optics EXPRESS

Ultrastructural features of collagen in thyroid carcinoma tissue observed by polarization second harmonic generation microscopy

Danielle Tokarz,[1] Richard Cisek,[2] Ahmad Golaraei,[2] Sylvia L. Asa,[3] Virginijus Barzda[2,4] and Brian C. Wilson[1,*]

[1]*Princess Margaret Cancer Centre, University Health Network, 101 College Street, Toronto, ON M5G 1L7, Canada*
[2]*Department of Physics, Institute for Optical Sciences and Department of Physical and Chemical Sciences, University of Toronto, 3359 Mississauga Road North, Mississauga, ON L5L 1C6, Canada*
[3]*University Health Network/University of Toronto, 200 Elizabeth Street, Toronto, ON M5G 2C4, Canada*
[4]*virgis.barzda@utoronto.ca*
[*]*wilson@uhn.utoronto.ca*

Abstract: Changes in collagen ultrastructure between malignant and normal human thyroid tissue were investigated *ex vivo* using polarization second harmonic generation (SHG) microscopy. The second-order nonlinear optical susceptibility tensor component ratio and the degree of linear polarization (DOLP) of the SHG signal were measured. The ratio values are related to the collagen ultrastructure, while DOLP indicates the relative amount of coherent signal and incoherent scattering of SHG. Increase in ratio values and decrease in DOLP were observed for tumor tissue compared to normal thyroid, indicating higher ultrastructural disorder in tumor collagen.

OCIS codes: (180.4315) Nonlinear microscopy; (170.3880) Medical and biological imaging; (170.4730) Optical pathology; (170.6935) Tissue characterization.

References and links

1. American Cancer Society, *Cancer Facts & Figs. 2015* (American Cancer Society, Atlanta, GA, USA, 2015).
2. S. Liu, R. Semenciw, A. M. Ugnat, and Y. Mao, "Increasing thyroid cancer incidence in Canada, 1970-1996: time trends and age-period-cohort effects," Br. J. Cancer **85**(9), 1335–1339 (2001).
3. S. A. Hundahl, I. D. Fleming, A. M. Fremgen, and H. R. Menck, "A national cancer data base report on 53,856 cases of thyroid carcinoma treated in the U.S., 1985–1995," Cancer **83**(12), 2638–2648 (1998).
4. V. A. Livolsi and S. L. Asa, "The demise of follicular carcinoma of the thyroid gland," Thyroid **4**(2), 233–236 (1994).
5. R. V. Lloyd, L. A. Erickson, M. B. Casey, K. Y. Lam, C. M. Lohse, S. L. Asa, J. K. Chan, R. A. DeLellis, H. R. Harach, K. Kakudo, V. A. LiVolsi, J. Rosai, T. J. Sebo, M. Sobrinho-Simoes, B. M. Wenig, and M. E. Lae, "Observer variation in the diagnosis of follicular variant of papillary thyroid carcinoma," Am. J. Surg. Pathol. **28**(10), 1336–1340 (2004).
6. T. M. Elsheikh, S. L. Asa, J. K. Chan, R. A. DeLellis, C. S. Heffess, V. A. LiVolsi, and B. M. Wenig, "Interobserver and intraobserver variation among experts in the diagnosis of thyroid follicular lesions with borderline nuclear features of papillary carcinoma," Am. J. Clin. Pathol. **130**(5), 736–744 (2008).
7. A. Golaraei, R. Cisek, S. Krouglov, R. Navab, C. Niu, S. Sakashita, K. Yasufuku, M.-S. Tsao, B. C. Wilson, and V. Barzda, "Characterization of collagen in non-small cell lung carcinoma with second harmonic polarization microscopy," Biomed. Opt. Express **5**(10), 3562–3567 (2014).
8. R. Ambekar, T.-Y. Lau, M. Walsh, R. Bhargava, and K. C. Toussaint, Jr., "Quantifying collagen structure in breast biopsies using second-harmonic generation imaging," Biomed. Opt. Express **3**(9), 2021–2035 (2012).
9. K. Tilbury, C. H. Lien, S. J. Chen, and P. J. Campagnola, "Differentiation of Col I and Col III isoforms in stromal models of ovarian cancer by analysis of second harmonic generation polarization and emission directionality," Biophys. J. **106**(2), 354–365 (2014).
10. A. Major, R. Cisek, D. Sandkuijl, and V. Barzda, "Femtosecond Yb:KGd(WO4)(2) laser with > 100 nJ of pulse energy," Laser Phys. Lett. **6**(4), 272–274 (2009).
11. D. Sandkuijl, A. E. Tuer, D. Tokarz, J. E. Sipe, and V. Barzda, "Numercial second- and third-harmonic generation microscopy," J. Opt. Soc. Am. B **30**(2), 382–395 (2013).

#243150 Received 16 Jun 2015; revised 6 Aug 2015; accepted 10 Aug 2015; published 21 Aug 2015

12. A. E. Tuer, M. K. Akens, S. Krouglov, D. Sandkuijl, B. C. Wilson, C. M. Whyne, and V. Barzda, "Hierarchical model of fibrillar collagen organization for interpreting the second-order susceptibility tensors in biological tissue," Biophys. J. **103**(10), 2093–2105 (2012).
13. A. Deniset-Besseau, J. Duboisset, E. Benichou, F. Hache, P.-F. Brevet, and M.-C. Schanne-Klein, "Measurement of the second-order hyperpolarizability of the collagen triple helix and determination of its physical origin," J. Phys. Chem. B **113**(40), 13437–13445 (2009).
14. P. J. Su, W. L. Chen, Y. F. Chen, and C. Y. Dong, "Determination of collagen nanostructure from second-order susceptibility tensor analysis," Biophys. J. **100**(8), 2053–2062 (2011).
15. M. Samim, S. Krouglov, and V. Barzda, "Double Stokes Mueller polarimetry of second-harmonic generation in ordered molecular structures," J. Opt. Soc. Am. B **32**(3), 451–461 (2015).
16. A. Tuer, D. Tokarz, N. Prent, R. Cisek, J. Alami, D. J. Dumont, L. Bakueva, J. Rowlands, and V. Barzda, "Nonlinear multicontrast microscopy of hematoxylin-and-eosin-stained histological sections," J. Biomed. Opt. **15**(2), 026018 (2010).
17. T. J. Wess, "Collagen fibril form and function," Adv. Protein Chem. **70**, 341–374 (2005).
18. D. Tokarz, R. Cisek, O. El-Ansari, G. S. Espie, U. Fekl, and V. Barzda, "Organization of astaxanthin within oil bodies of *Haematococcus pluvialis* studied with polarization-dependent harmonic generation microscopy," PLoS One **9**(9), e107804 (2014).
19. N. Mazumder, J. Qiu, M. R. Foreman, C. M. Romero, C. W. Hu, H. R. Tsai, P. Török, and F. J. Kao, "Polarization-resolved second harmonic generation microscopy with a four-channel Stokes-polarimeter," Opt. Express **20**(13), 14090–14099 (2012).
20. F. Légaré, C. L. Evans, F. Ganikhanov, and X. S. Xie, "Towards CARS endoscopy," Opt. Express **14**(10), 4427–4432 (2006).
21. M. Ji, D. A. Orringer, C. W. Freudiger, S. Ramkissoon, X. Liu, D. Lau, A. J. Golby, I. Norton, M. Hayashi, N. Y. R. Agar, G. S. Young, C. Spino, S. Santagata, S. Camelo-Piragua, K. L. Ligon, O. Sagher, and X. S. Xie, "Rapid, label-free detection of brain tumors with stimulated Raman scattering microscopy," Sci. Transl. Med. **5**(201), 201ra119 (2013).

1. Introduction

Thyroid cancers are the most common malignancy of the endocrine organs [1] and the incidence rate of differentiated thyroid cancers has increased significantly over the past decade [2]. Papillary thyroid carcinoma is the most prevalent form, accounting for 85-90% of all thyroid cancer cases, while follicular thyroid carcinoma accounts for <10% [3, 4]. Most papillary and follicular thyroid cancers can be treated successfully when diagnosed early. Diagnosis of thyroid cancer is confirmed by visualizing stained thyroid tissue with bright-field microscopy. However, morphological interpretation of tissue by standard histopathology can be controversial with significant inter-observer variability [5, 6], so that novel automated technologies with high spatial resolution and improved disease specificity are needed to aid pathologists in identifying cancer on biopsy or surgical resection sections.

Extracellular matrix (ECM) development is often deregulated and becomes disorganized during cancer initiation and progression. In principle then, cancer diagnosis can be improved by developing a technique that identifies and quantifies structural details in the ECM. Since collagen is the most abundant protein in the ECM and is known to have strong second harmonic generation (SHG) signals without staining, its content and spatial micro-distribution can be visualized by SHG microscopy [7]. Further, by applying polarization-sensitive measurements, the second-order nonlinear optical susceptibility tensor component ratio, $\chi^{(2)}{}_{ZZZ}{}'/\chi^{(2)}{}_{ZXX}{}'$, and the degree of linear polarization, DOLP, can be measured. These metrics provide additional information on the collagen ultrastructural characteristics that is complementary to the concentration and spatial distribution measures. Polarization-sensitive SHG microscopy has been previously applied to determine differences in normal and malignant breast tissue [8], models of ovarian cancer [9], and non-small cell lung carcinoma [7]. In this study, we use polarization-in, polarization-out (PIPO) SHG microscopy to investigate classical papillary thyroid carcinoma (cPTC) and follicular variant papillary thyroid carcinoma (FVPTC).

#243150 Received 16 Jun 2015; revised 6 Aug 2015; accepted 10 Aug 2015; published 21 Aug 2015

2. Materials and methods

2.1 Polarization-sensitive SHG measurements with a nonlinear optical microscope

For imaging, an in-house system consisting of a ytterbium-ion-doped potassium gadolinium tungstate (Yb:KGW) crystal-based laser oscillator operating at 1028 nm with 14.3 MHz repetition rate and ~450 fs pulse duration [10] was coupled to an in-house nonlinear optical microscope. Excitation was achieved with a 0.75 numerical aperture (NA) objective lens (Carl Zeiss, Thornwood, NY, USA), while emission occurred in the transmission geometry with a 0.85 NA objective (fabricated in-house). The high NA lenses are expected to produce ~5% overestimation of $\chi^{(2)}_{ZZZ}{}'/\chi^{(2)}_{ZXX}{}'$ [11]. We assume that the induced axial polarization component is negligible. The PIPO SHG measurement consisted of recording 81 images at different combinations of orientation angles by rotating a half-wave plate placed directly before the excitation objective lens, and a polarizer (analyzer) located after the collection objective before the detector, resulting in excitation and SHG polarization orientation ranges of −90° to 90° [12]. To ensure that the input beam is linearly polarized, a linear polarizer was placed directly before the half-wave plate, and there were no optical elements after the linear polarizer, such as dichroic or dielectric mirrors, that could affect the polarization state.

2.2 Polarization-sensitive SHG image analysis

A laboratory Cartesian coordinate system, *XYZ*, is defined such that *XZ* is the image plane and the laser propagates along the *Y*-direction. The average orientation of collagen fibers in a pixel is defined by modified spherical angles, α and δ, where α is the angle between the axis of the collagen fibers and their projection onto the image plane, while δ is the angle between the laboratory frame *Z* axis and that projection. The collagen fibers are associated with their own Cartesian coordinates, *xyz*, where the *z*-axis is oriented along the collagen fiber axis. The measured second-order nonlinear optical susceptibility tensor component ratio, $\chi^{(2)}_{ZZZ}{}'/\chi^{(2)}_{ZXX}{}'$, for a sample voxel that contains cylindrical fibers of collagen [13, 14] with an intrinsic second-order nonlinear optical susceptibility tensor component ratio, $\chi^{(2)}_{zzz}/\chi^{(2)}_{zxx}$, oriented at angles α and δ is given by [12]:

$$\frac{\chi^{(2),}_{ZZZ}}{\chi^{(2),}_{ZXX}} = \frac{\left(\frac{\chi^{(2)}_{zzz}}{\chi^{(2)}_{zxx}} - 3\right)\cos^2\alpha\cos^2\delta + 3}{\left(\frac{\chi^{(2)}_{zzz}}{\chi^{(2)}_{zxx}} - 3\right)\cos^2\alpha\sin^2\delta + 1}. \tag{1}$$

The $\chi^{(2)}_{ZZZ}{}'/\chi^{(2)}_{ZXX}{}'$ for each pixel of the SHG image is fitted to the PIPO SHG measurements, where the SHG intensity, $I_{2\omega}$, is expressed as a function of the orientation of linear polarization of the laser, $\theta'=\theta+\delta$, and the analyzer orientation, $\varphi'=\varphi+\delta$. *A* is the fitted noise and *B* is the fitted amplitude [12]. Thus:

$$I_{2\omega} = A + B\left(\sin\varphi'\sin 2\theta' + \cos\varphi'\sin^2\theta' + \frac{\chi^{(2),}_{ZZZ}}{\chi^{(2),}_{ZXX}}\cos\varphi'\cos^2\theta'\right)^2. \tag{2}$$

Equation (2) is valid for the case of cylindrical symmetry and birefringence can be neglected due to the minimal tissue thickness.

The polarization dependence of incoherent SHG (I_{incoh}) can be described by Eq. (2) at 4 orthogonal values of the fiber orientation δ, yielding:

$$I_{incoh} = \sum_{n=0}^{3} I_{2\omega}(\delta = n\pi/2) = \left(\frac{\chi^{(2),}_{ZZZ}}{\chi^{(2),}_{ZXX}} + 1\right)^2 \cos^2\left(\theta' - \varphi'\right) + \frac{1}{4}\left(\left(\frac{\chi^{(2),}_{ZZZ}}{\chi^{(2),}_{ZXX}}\right)^2 - 2\frac{\chi^{(2),}_{ZZZ}}{\chi^{(2),}_{ZXX}} + 5\right). \tag{3}$$

From the PIPO SHG meausrements, the DOLP of the outgoing SHG was obtained from:

#243150 Received 16 Jun 2015; revised 6 Aug 2015; accepted 10 Aug 2015; published 21 Aug 2015

$$\mathrm{DOLP} = \frac{\sqrt{s_1^2 + s_2^2}}{s_0}, \tag{4}$$

where s_0, s_1 and s_2 are Stokes parameters describing the SHG polarization: specifically, $s_0 = I_0 + I_{90}$, $s_1 = I_0 - I_{90}$, and $s_2 = I_{45} - I_{-45}$, where I_a is the SHG intensity at the analyzer angle a. According to double Stokes Mueller polarimetry [15], a measurement of the DOLP depends on the angle between the incident polarization of the laser and the measured collagen fiber angle (δ). When the laser polarization orientation is 90° from the collagen axis, SHG intensity is reduced and noise dominates the signal, rendering the DOLP unreliable. Nevertheless, meaningful data were obtained by averaging 16 independent DOLP measurements, 2 at each orientation of the incident laser polarization (0°, 22.5°, 45°, 67.5°, 90°, 112.5°, 135°, 157.5°).

2.3 Sample preparation

Histological sections of tumor and non-tumorous thyroid tissue were obtained according to an institutionally-approved protocol (University Health Network, Toronto). Thin (5 μm) tissue sections were cut from formalin-fixed, paraffin-embedded tissue blocks, mounted on glass slides and stained with hematoxylin and eosin (H&E). The whole sections were imaged with a bright-field microscope scanner (Aperio Whole Slide Scanner: Leica Biosystems, Germany).

Assessment of both the tissue architecture and cytology of tumor cells was performed by an expert pathologist (S.L.A.) for identification of tumor and non-tumor regions of interest on the bright-field images. In H&E stained tissues, collagen gives rise to strong SHG signals [16], so that PIPO SHG scans were subsequently performed on 110 × 110 μm regions. As a control and to correct for possible photobleaching, the sample was periodically re-scanned at the initial polarizer and analyzer settings. In each sample slide, at least 2 regions of interest were imaged. In total, 16 areas in 5 patients with non-tumorous thyroid, 48 areas from 10 patients with cPTC tumors and 58 areas from 17 patients with FVPTC tumors were imaged. Two-tailed t-tests were conducted considering the number of patients imaged.

3. Results

PIPO SHG microscopy was used to investigate ultrastructural changes in collagen between follicles in non-tumorous thyroid tissue and FVPTCs as well as collagen found in the papillae of cPTC. Bright field microscopy images of the H&E stained tissue sections are shown in Fig. 1(a), 1(g), 1(m) and the corresponding areas imaged with PIPO SHG microscopy in Fig. 1(b), 1(h), 1(n) are also indicated. The $\chi^{(2)}{}_{ZZZ}'/\chi^{(2)}{}_{ZXX}'$ for each pixel in the SHG images in Fig. 1(b), 1(h), 1(n) was extracted by fitting the PIPO SHG intensity data with Eq. (2).

Table 1. Average (± standard error) values of $\chi^{(2)}{}_{ZZZ}'/\chi^{(2)}{}_{ZXX}'$, the FWHM, the isotropic fraction and the DOLP for normal thyroid and tumor tissues.

Tissue	Samples	Areas	$\chi^{(2)}{}_{ZZZ}'/\chi^{(2)}{}_{ZXX}'$	FWHM	ψ (%)	DOLP
Nontumor	5	16	2.15 ± 0.01	0.69 ± 0.02	18 ± 3	0.69 ± 0.02
FVPTC	17	58	2.26 ± 0.02	0.63 ± 0.02	44 ± 5	0.44 ± 0.02
cPTC	10	48	2.23 ± 0.02	0.64 ± 0.02	45 ± 4	0.51 ± 0.02

The $\chi^{(2)}{}_{ZZZ}'/\chi^{(2)}{}_{ZXX}'$ values for each pixel in Fig. 1(b), 1(h), 1(n) are displayed as a color-coded map in Fig. 1(c), 1(i), 1(o), where the $\chi^{(2)}{}_{ZZZ}'/\chi^{(2)}{}_{ZXX}'$ values are represented from blue to red. Figure 1(d), 1(j), 1(p) shows $\chi^{(2)}{}_{ZZZ}'/\chi^{(2)}{}_{ZXX}'$ occurrence frequency histograms for all the pixels in the images and the average $\chi^{(2)}{}_{ZZZ}'/\chi^{(2)}{}_{ZXX}'$ resulting from a single Gaussian fit to these histograms is given in Table 1. The difference between the average $\chi^{(2)}{}_{ZZZ}'/\chi^{(2)}{}_{ZXX}'$ of non-tumor thyroid tissue and FVPTC and cPTC were 0.11 ± 0.03 and 0.08 ± 0.02, respectively and these differences are statistically significant ($p<0.01$ and <0.05, respectively). The average full width at half maximum (FWHM) of the $\chi^{(2)}{}_{ZZZ}'/\chi^{(2)}{}_{ZXX}'$ frequency histograms of non-tumorous thyroid tissue also differed from those of FVPTC and

#243150 Received 16 Jun 2015; revised 6 Aug 2015; accepted 10 Aug 2015; published 21 Aug 2015

cPTC by 0.06 ± 0.03 and 0.05 ± 0.03, respectively, but these differences were not statistically significant ($p<0.30$ and <0.10).

Many pixels in FVPTC and cPTC samples (Fig. 1(h), 1(n)) could not be fit well with Eq. (2) because they had similar elongated PIPO SHG contour plots, (compare typical elongated contour plots Fig. 2(b), 2(c) to typical normal thyroid Fig. 2(a)). Elongation represents incoherent SHG contribution independent of the polarizer angle, therefore an additional term representing incoherent SHG from Eq. (3) was added to Eq. (2) for fitting the experimental PIPO SHG contour plots:

$$I'_{2\omega} = A + B\left(\sin\varphi'\sin 2\theta' + \cos\varphi'\sin^2\theta' + \frac{\chi^{(2)\prime}_{ZZZ}}{\chi^{(2)\prime}_{ZXX}}\cos\varphi'\cos^2\theta'\right)^2 + C\cos^2\left(\theta' - \varphi'\right). \quad (5)$$

The added term, $C\cos^2(\theta'-\varphi')$, allowed for a better fit to the data, as shown in Fig. 2(e), 2(f). All the data were then re-fitted to Eq. (5) and a new metric ψ was devised to quantify the percentage of fitted pixels per image that required a significant isotropic term:

$$\psi = \frac{N'}{N+N'}, \quad (6)$$

where N and N' represent the number of pixels in each area that had good fit with Eqs. (2) and (5), respectively, determined by a goodness of fit linear regression parameter, $R^2>0.8$. Average ψ values in Table 1 verify the observation that FVPTC and cPTC tissues contain more elongated PIPO profiles than normal tissue ($p<0.01$ and <0.05, respectively). ψ shows the percentage of the affected collagenous area that contains partly disordered collagen ultrastructure.

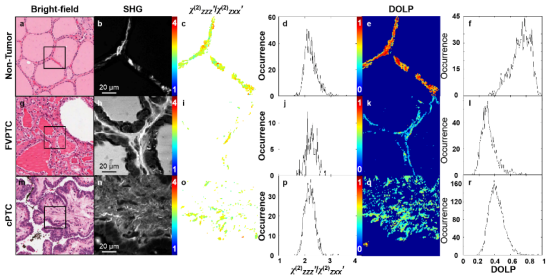

Fig. 1. Bright field microscopy images of H&E stained (a) non-tumorous and (g, m) cancerous thyroid tissue sections, where the black boxes indicate 110 × 110 μm regions of interest imaged by PIPO SHG microscopy in panels (b, h, n). The $\chi^{(2)}_{ZZZ}'/\chi^{(2)}_{ZXX}'$ values were calculated for each pixel from Eq. (2), and are displayed as color-coded maps in panels (c, i, o), where blue indicates a $\chi^{(2)}_{ZZZ}'/\chi^{(2)}_{ZXX}'$ of 1 and red indicates 4. The frequency histograms of the $\chi^{(2)}_{ZZZ}'/\chi^{(2)}_{ZXX}'$ values for all the pixels are plotted in panels (d, j, p). From PIPO SHG microscopy data, DOLP values were also extracted for each pixel and are displayed as color-coded maps in panels (e, k, q), where blue indicates a DOLP of 0 and red indicates 1. Frequency histograms of the DOLP values for all the pixels are plotted in panels (f, l, r).

The isotropic SHG contribution can also be characterized by calculating the DOLP for each pixel using Eq. (4), as in Fig. 1(e), 1(k), 1(q). While DOLP values are calculated for all pixels with intense SHG, reliable $\chi^{(2)}_{ZZZ}'/\chi^{(2)}_{ZXX}'$ values are only generated from good fits with Eq. (2), which explains why there are less pixels in $\chi^{(2)}_{ZZZ}'/\chi^{(2)}_{ZXX}'$ images of cPTC and FVPTC as compared with DOLP images (Fig. 1(i), 1(o) versus 1(k), 1(q)). The DOLP frequency histograms in Fig. 1(f), 1(l), 1(r) and the mean DOLP values resulting from a single Gaussian fit to these histograms are also given in Table 1. The differences between the average DOLP of non-tumorous thyroid tissue and FVPTC and cPTC were 0.25 ± 0.03 and 0.18 ± 0.03, respectively, which are statistically significant ($p<0.001$ and <0.002, respectively).

#243150 Received 16 Jun 2015; revised 6 Aug 2015; accepted 10 Aug 2015; published 21 Aug 2015

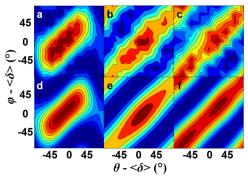

Fig. 2. Representative PIPO SHG contour plots from individual pixels of various images: (a) normal thyroid, (b) FVPTC and (c) cPTC. The SHG intensity is represented on a false-color scale, where blue corresponds to 0 and red represents maximum intensity. Corresponding fit with Eq. (2) is in (d) and with Eq. (5) in (e, f).

4. Discussion

Significant changes in $\chi^{(2)}_{ZZZ}'/\chi^{(2)}_{ZXX}'$ and DOLP values were observed between tumor and non-tumorous thyroid tissues. Changes in $\chi^{(2)}_{ZZZ}'/\chi^{(2)}_{ZXX}'$ for collagen have previously been ascribed to possible alterations in the helical angle of the triple helix and/or the arrangement of the triple helices into fibrils and fibers and/or the distribution of fibrils and fibers within the laser focal volume [7, 17]. Increase in $\chi^{(2)}_{ZZZ}'/\chi^{(2)}_{ZXX}'$ is attributed to increased distribution of fibers and fibrils in the focal volume, which can be understood from Eq. (1) wherein larger lateral (δ) or axial (α) variations increase the measured $\chi^{(2)}_{ZZZ}'/\chi^{(2)}_{ZXX}'$ values when $\chi^{(2)}_{ZZZ}'/\chi^{(2)}_{ZXX}'<3$. Hence, the increased $\chi^{(2)}_{ZZZ}'/\chi^{(2)}_{ZXX}'$ in thyroid tumor tissue may then be due to an increase in the fibril orientation distribution, indicating greater fibril disorder.

The isotropic SHG contribution is reminiscent of the PIPO THG pattern produced by isotropic media [18]. Such media cannot produce coherent SHG, so that the observed contribution is attributed to incoherent hyper-Rayleigh scattered SHG from disordered collagen fibrils and small collagen fibril segments within the voxel volume. The DOLP was also calculated for each pixel to reflect the isotropic SHG contribution to the polarization plots. The SHG signals from non-tumorous thyroid tissue and tumors differed significantly in their DOLP values, indicating that tumor tissue has a greater degree of ultrastructural collagen disorder. This conclusion is somewhat similar to a previous study of the DOLP of SHG from collagen type I gels formed from bovine tendon [19]. Generally, care must be taken in interpreting DOLP data, since the circular polarization component can alter the DOLP due to SHG radiation propagation through a birefringent sample. However, since the samples used were optically thin (5 μm), the influence of birefringence and scattering due to SHG propagation through the tissue can be considered to be negligible.

In conclusion, the decrease in the DOLP values of cancerous thyroid tissue indicates that collagen becomes increasingly disordered in diseased states. The increase in $\chi^{(2)}_{ZZZ}'/\chi^{(2)}_{ZXX}'$ also indicates that the collagen structure becomes increasingly disordered. One caveat in these findings is that to date the analysis has not included samples from patients with Graves' disease in which the thyroid develops papillae or nodular hyperplasia where stromal changes occur. This will be necessary to validate the use of PIPO SHG microscopy to complement standard histopathology to improve the accuracy of thyroid cancer diagnosis and staging. There are also recent reports of implementing various nonlinear optical technqiues *in vivo*, either endoscopically (e.g. coherent anti-Stokes Raman, as in ref. [20]) or intraoperatively to localize tumor margins (e.g. stimulated Raman, as in ref. [21]).

Acknowledgments

This work was supported by the Natural Sciences and Engineering Research Council of Canada and the Canadian Institutes of Health Research through a CHRP grant (CPG-134752 and CHRPJ 462842-14).

#243150 Received 16 Jun 2015; revised 6 Aug 2015; accepted 10 Aug 2015; published 21 Aug 2015